IJFANS INTERNATIONAL JOURNAL OF FOOD AND NUTRITIONAL SCIENCES
ISSN PRINT 2319 1775 Online 2320 7876
 UGC CARE Listed (Group -I) Journal Volume 12, Iss 04, 2023

EXPLORATION OF POTENTIAL ANTITUBERCULOSIS COMPOUNDS IN ASTRAEUS ASIATICUS VIA MOLECULAR DOCKING WITH MMPL3

Samay Tirkey[1], Srishti Verma[2], Prof. Aditi Niyogi Poddar[3], Dr. Kamlesh Kumar Shukla[4]
[1,3]School of Studies in Life Science, Pt. Ravishankar Shukla University Raipur (C.G.), India
[2,4]School of Studies in Biotechnology, Pt. Ravishankar Shukla University, Raipur (C.G.), India

Abstract

Tuberculosis (TB) remains a global health challenge by the rise of drug-resistant Mycobacterium tuberculosis strains. Current treatments suffer from suboptimal efficacy and toxicity, necessitating new antitubercular agents. This study explores the potential of natural products from the mushroom Astraeus asiaticus. We conducted molecular docking studies of 64 metabolites against the MmpL3 protein, revealing several compounds with promising inhibitory potential. Metabolites with binding affinities between -6.5 to -8.7 using AutoDock Vina, were further analyzed using the SwissADME tool for drug-likeness and pharmacokinetic properties. Notably, compounds such as (E)-3-benzylidene-4-methyl-3, 4-dihydro-1H-benzo[e] [1,4] diazepine-2,5-dione ($C_{17}H_{14}N_2O_2$) and (13S) – 3 – hydroxy – 13 – methyl - 7, 8, 9, 11, 12, 13, 15, 16 – octahydro - 6H – cyclopenta [a] phenanthrene – 17 (14H) - one ($C_{18}H_{22}O_2$) showed high binding affinity, stability, and favorable drug-likeness property. These findings suggest A. asiaticus as a promising natural source for new antituberculosis agents targeting MmpL3, providing a foundation for further in vitro and in vivo validation.

Keywords: Antituberculosis, Astraeus asiaticus, MmpL3 protein, Molecular Docking, Bioactive compounds

Introduction

Tuberculosis (TB) remains a significant global health challenge, now recognized as the second leading cause of death from a single infectious agent, following COVID-19. The recent coronavirus pandemic exacerbates this situation, threatening to undermine previous advances in TB control. According to the World Health Organization (WHO), 10 million people developed TB in 2020, with the disease claiming 1.5 million lives, an increase from 1.4 million deaths in 2019 (Liang et al., 2023). The rise of drug-resistant M. tuberculosis strains has significantly impeded global efforts to eradicate TB. Existing TB treatment regimens, which rely predominantly on decades-old medications, suffer from issues such as suboptimal efficacy, toxicity, extended duration, and poor patient adherence, all of which contribute to the development of drug-resistant TB (Bendre et al., 2021).

The standard treatment for drug-susceptible TB involves an intensive 2-month phase with a combination of four first-line drugs (isoniazid, rifampicin, ethambutol, and pyrazinamide), followed by a continuation phase of at least 4 months with isoniazid and rifampicin to target

dormant bacilli (Baye et al., 2018; Liang et al., 2023). However, therapies for multidrug-resistant (MDR), pre-extensively drug-resistant (pre-XDR), and extensively drug-resistant (XDR) TB are more toxic, costly, and less effective (Silva et al., 2018). Global data reveals unsatisfactory success rates for treating drug-resistant TB (approximately 57% for MDR- or rifampicin-resistant TB) compared to drug-susceptible TB cases (around 85%) (Traoré et al., 2022).

Despite the availability of TB antibiotics providing some relief, they are insufficient to completely overcome the resilience of M. tuberculosis, indicating a significant unmet medical need (Baye et al., 2018). The global clinical development pipeline for potential anti-TB agents, reflecting 22 drugs in 2020 and updated to 25 in August 2021, continues to expand (Theuretzbacher et al., 2020). Two agents, bedaquiline and delamanid, have recently gained accelerated approval for treating drug-resistant TB forms (Silva et al., 2018). The WHO has also endorsed pretomanid, a nitroimidazole developed by TB Alliance, for the treatment of fluoroquinolone-resistant MDR-TB (pre-XDR) in combination with bedaquiline and linezolid, under operational research conditions. Other drugs in the pipeline include repurposed medications like levofloxacin and novel compounds such as the diarylquinoline TBAJ-876 (a 3,5-dialkoxypyridine analogue of bedaquiline) (Sarathy et al., 2020), ethylenediamine SQ109 (Parida et al., 2015), and benzothiazinone BTZ043 along with its optimized analogue macozinone (Wang et al., 2020). These candidates target previously unexplored pathways and introduce new chemical classes.

In light of the challenges posed by drug-resistant TB and the limitations of current treatments, there is an urgent need for innovative and intensified drug discovery efforts. One promising avenue involves the exploration of natural products for their potential antituberculosis properties. Mushrooms, particularly those from the genus Astraeus, have gained attention for their diverse bioactive compounds (Arpha et al., 2012). A. asiaticus, a mushroom species known for its medicinal properties, has shown potential in various therapeutic areas (Biswas et al., 2017). In this study, we focus on the in-silico analysis of 64 metabolites extracted and identified by the methanolic extract of A. asiaticus for their antituberculosis potential.

Using molecular docking, these metabolites were evaluated against the MmpL3 protein, a critical component of the M. tuberculosis cell wall synthesis machinery. This protein is essential for the transport of mycolic acids, which are vital for the bacterial cell wall integrity and survival (Li et al., 2016). By targeting MmpL3, we aim to identify novel inhibitors that can potentially overcome the resistance mechanisms of M. tuberculosis. This research seeks to contribute to the growing body of knowledge on natural product-derived antituberculosis agents and to provide a foundation for the development of new therapeutic strategies against TB.

Methodology

Sample Collection and Preparation:

Fresh fruiting bodies of A. asiaticus were collected from the forest. The collected mushrooms were air-dried at a temperature range of 55-60°C until they reached complete dry. This drying process

typically took 1-2 days to complete removal of moisture (Sun et al., 2016) . The dried mushroom samples were then ground into a fine powder using a mechanical grinder by maintaining the temperature in a tolerable range (Lakshmipathy, 2013). The powdered sample was stored in airtight containers to prevent moisture absorption until further analysis and the containers were stored for long time in -20°C for.

Metabolic Extraction:

The dried mushroom powder was subjected to solvent based extraction using methanol as the solvent. For this, 10 grams of mushroom powder was soaked in 200 mL of methanol (1:20). The mixture was allowed to stand for 48 hours with occasional shaking to facilitate the extraction process. After the extraction, the mixture was filtered using Whatman No. 1 filter paper to separate the methanol extract from the residual mushroom powder (Al-obaidy & Esmaeel, 2021).

The methanol extract was concentrated by evaporating the solvent using a rotary evaporator set at 42°C under reduced pressure. The resultant concentrated extract was dried completely to obtain a solid residue. The dried extract residue was re-dissolved in methanol to prepare a stock solution with a concentration of 100 mg/mL (Tan et al., 2018). This stock solution was stored at 4°C until further analysis.

OHRLCMS (Orbitrap High-Resolution liquid Chromatography-Mass Spectrometry) Analysis:

The methanol extract was subjected to OHRLCMS for the profiling of small molecules. The analysis was carried out at the Sophisticated Analytical Instrumentation Facility (SAIF) Indian Institute of Technology (IIT) Bombay. A Thermo Scientific Vanquish UHPLC system was utilized with a total runtime of 35 minutes and a column compartment temperature of 40°C. The UV detection settings were a time constant of 0.12 seconds and a data collection rate of 10 Hz, while the autosampler was maintained at 4°C. The mobile phase solvents were 0.1% formic acid in water (A), methanol (B), and acetonitrile (C), with a pressure range of 0-1034 bar and a constant flow rate of 0.300 ml/min. The identified compounds were cataloged based on their retention times and mass-to-charge (m/z) ratios.

In Silico Antitubercular Activity

Compound Identification and Preparation:

The identified compounds from the HRLCMS analysis were drawn using ChemDraw Ultra 12.0 software. The chemical structures were verified and saved for further in silico analysis.

Protein Preparation:

The protein structure of the membrane protein MmpL3 (PDB ID: 7nvh) was downloaded from the Protein Data Bank (PDB) (Rayasam, 2014). The protein structure was prepared for docking studies

ISSN PRINT 2319 1775 Online 2320 7876
 UGC CARE Listed (Group -I) Journal Volume 12, Iss 04, 2023

by using Discovery Studio Visualizer software, which included the removal of water molecules, addition of hydrogen atoms, and optimization of the protein structure.

Molecular Docking:

The prepared protein and the drawn compounds were subjected to molecular docking studies using AutoDock Vina integrated into the PyRx software platform (Dallakyan & Olson, 2015). The docking parameters were set, and the binding site of the protein was defined based on the active site information. Each compound was docked into the binding site of MmpL3 to predict the binding affinity and interaction pattern (Azam et al., 2015).

Interaction Analysis:

The interaction patterns between the protein and the ligands were analyzed using Discovery Studio Visualizer software. Key interactions such as hydrogen bonds, hydrophobic interactions, and electrostatic interactions were identified and visualized (Jejurikar & Rohane, 2021).

Drug-likeness and pharmacokinetic properties:

To evaluate the drug-likeness and pharmacokinetic properties of the metabolites extracted from A. asiaticus, the SwissADME web tool (http://www.swissadme.ch/) was utilized.

Statistical Analysis & Graphical Representation:

IBM SPSS Statistics 20 software was used for statistical analysis of the docking results. The data obtained from the docking studies and statistical analysis were graphically represented using Origin Pro 2016 software.

Results and discussion

Metabolic extraction:

O-HRLCMS analysis of the mushroom extract led to the identification of a diverse array of compounds. Their structures are represented in Figure 1 & Figure 2, and the detailed list of the identified compounds is presented in Table 1, which includes their molecular formulas and names. The identified compounds reflect the complex and diverse biochemical nature of the mushroom extract. The presence of various amino acids, vitamins, phenolic acids, and other bioactive molecules underscores the potential health benefits and therapeutic applications of the mushroom. These findings suggest that the mushroom extract may offer a wide range of bioactive properties, including antibiotic, antioxidant, anti-inflammatory, and metabolic regulatory activities.

ISSN PRINT 2319 1775 Online 2320 7876
 UGC CARE Listed (Group -I) Journal Volume 12, Iss 04, 2023

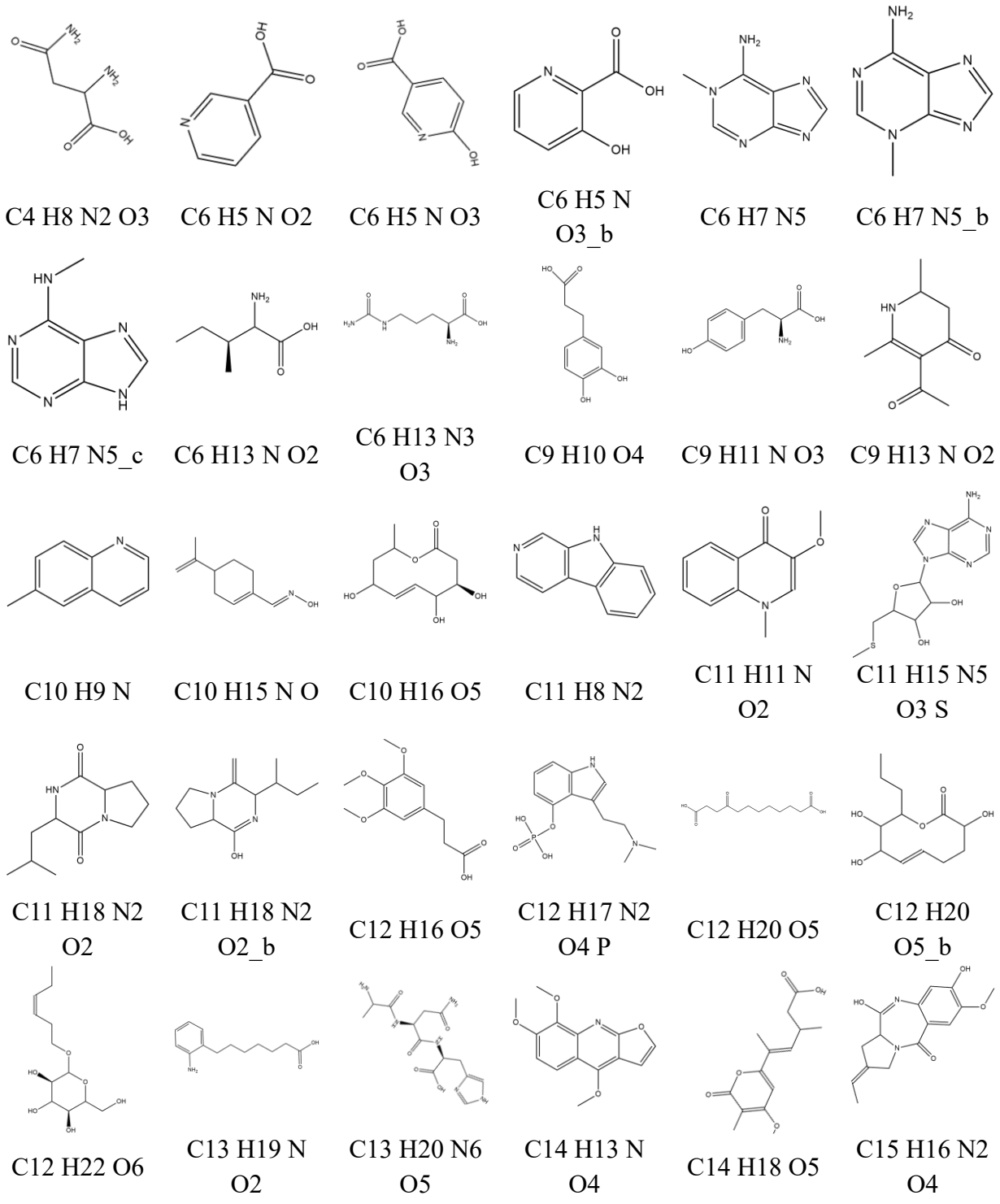

Figure 1 Structural representation of compounds identified in the A. asiaticus. The structures are depicted along with their corresponding molecular formulas. Compounds with the same molecular formula but different structures are indicated with the letters a, b, c, and d representing structural isomers.

ISSN PRINT 2319 1775 Online 2320 7876
 UGC CARE Listed (Group -I) Journal Volume 12, Iss 04, 2023

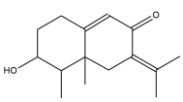
C15 H22 O2

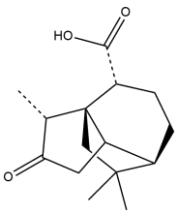
C15 H22 O3

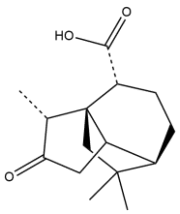
C15 H22 O3_b

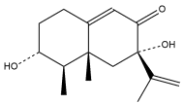
C15 H22 O3_c

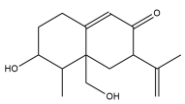
C15 H22 O3_d

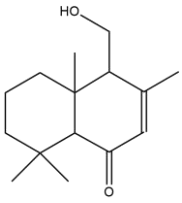
C15 H24 O2

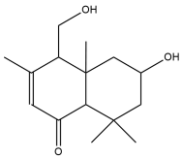
C15 H24 O3

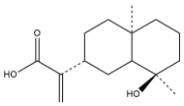
C15 H24 O3_b

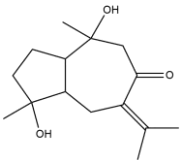
C15 H24 O3_c

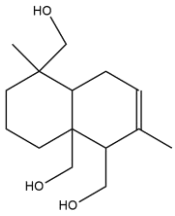
C15 H26 O3

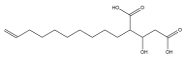
C15 H26 O5

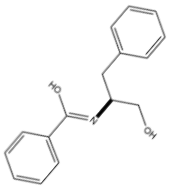
C16 H17 N O2

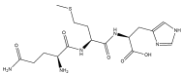
C16 H26 N6 O5 S

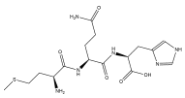
C16 H26 N6 O5 S_b

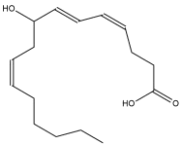
C16 H26 O3

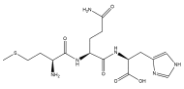
C16H26N6O 5S

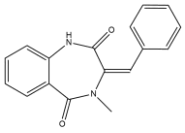
C17 H14 N2 O2

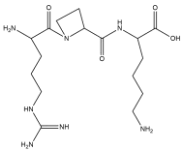
C17 H33 N7 O4

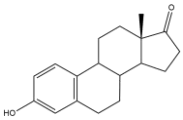
C18 H22 O2

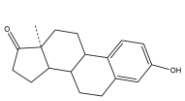
C18 H22 O2_b

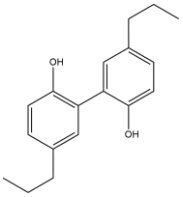
C18 H22 O2_c

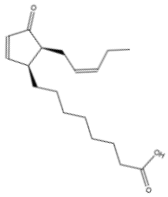
C18 H28 O3

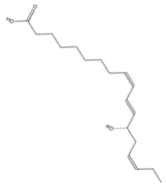
C18 H30 O3

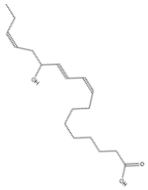
C18 H30 O3_b

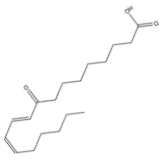
C18 H30 O3_c

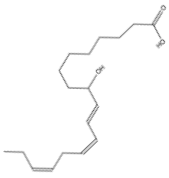
C18 H30 O3_d

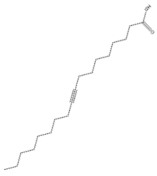
C18 H32 O2

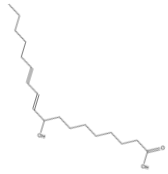
C18 H32 O3

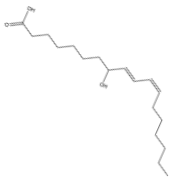
C18 H32 O3_b

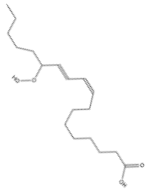
C18 H32 O4

ISSN PRINT 2319 1775 Online 2320 7876
 UGC CARE Listed (Group -I) Journal Volume 12, Iss 04, 2023

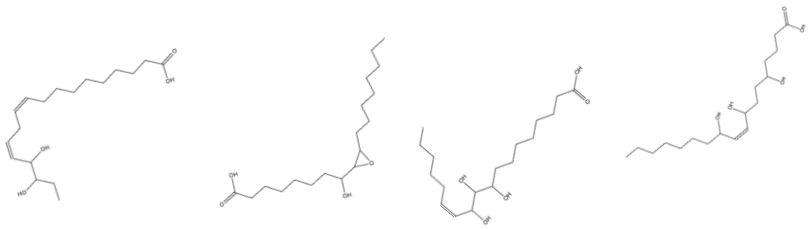

C18 H32 O4_b | C18 H34 O4 | C18 H34 O5 | C18 H34 O5_b

Figure 2 Structural representation of compounds identified in the A. asiaticus. The structures are depicted along with their corresponding molecular formulas. Compounds with the same molecular formula but different structures are indicated with the letters a, b, c, and d representing structural isomers.

Table 1 List of compounds identified in the methanolic extract of A. asiaticus by HRLCMS, including their molecular formulas and names.

S. No.	Formula	Name
1	C4 H8 N2 O3	2,4-diamino-4-oxobutanoic acid
2	C6 H5 N O2	nicotinic acid
3	C6 H5 N O3	6-Hydroxynicotinic acid
4	C6 H5 N O3_b	3-Hydroxypicolinic acid
5	C6 H7 N5	1-methyladenine
6	C6 H7 N5_b	3-methyladenine
7	C6 H7 N5_c	N6-methyladenine
8	C6 H13 N O2	(3S)-2-amino-3-methylpentanoic acid
9	C6 H13 N3 O3	L-(+)-Citrulline
10	C9 H10 O4	3-(3,4-dihydroxyphenyl) propanoic acid
11	C9 H11 N O3	L-Tyrosine
12	C9 H13 N O2	5-acetyl-2,6-dimethyl-2,3-dihydropyridin-4(1H)-one
13	C10 H9 N	6-Methylquinoline
14	C10 H15 N O	(E)-4-(prop-1-en-2-yl) cyclohex-1-enecarbaldehyde oxime (Perillartine)
15	C10 H16 O5	(4S,5S,8S,10R)-4,5,8-trihydroxy-10-methyl-3,4,5,8,9, 10-hexahydro-2Hoxecin-2-one
16	C11 H8 N2	9H-pyrido[3,4-b] indole
17	C11 H11 N O2	3-methoxy-1-methylquinolin-4(1H)-one
18	C11 H15 N5 O3 S	2-(6-amino-9H-purin-9-yl)-5-((methylthio) methyl) tetrahydrofuran-3,4-diol

19	C11 H18 N2 O2	3-isobutylhexahydropyrrolo[1,2-a]pyrazine-1,4-dione
20	C11 H18 N2 O2_b	3-(sec-butyl)-4-methylene-3,4,6,7,8,8a-hexahydropyrrolo[1,2-a]pyrazin-1-ol
21	C12 H16 O5	3-(3,4,5-trimethoxyphenyl) propanoic acid
22	C12 H17 N2 O4 P	3-(2-(dimethyl amino) ethyl)-1H-indol-4-yl dihydrogen phosphate
23	C12 H20 O5	4-oxododecanedioic acid
24	C12 H20 O5_b	3,8,9-trihydroxy-10-propyl-3,4,5,8,9,10-hexahydro-2Hoxecin-2-one
25	C12 H22 O6	(3R,5S)-2-((Z)-hex-3-en-1-yloxy)-6-(hydroxymethyl) tetrahydro-2H-pyran-3,4,5-triol
26	C13 H19 N O2	7-(2-aminophenyl) heptanoic acid
27	C13 H20 N6 O5	(2S)-2-((2S)-4-amino-2-(2-aminopropanamido)-4-oxobutanamido)-3-(1H-imidazol-4-yl) propanoic acid
28	C14 H13 N O4	4,7,8-trimethoxyfuro[2,3-b] quinoline
29	C14 H18 O5	(E)-5-(4-methoxy-3-methyl-2-oxo-2H-pyran-6-yl)-3-methylhex-4-enoic acid
30	C15 H16 N2 O4	(Z)-2-ethylidene-8,11-dihydroxy-7-methoxy-2,3-dihydro-1H-benzo[e]pyrrolo[1,2-a] [1,4] diazepin-5(11aH)-one
31	C15 H22 O2	6-hydroxy-4a,5-dimethyl-3-(propan-2-ylidene)-4,4a,5,6,7,8-hexahydronaphthalen-2(3H)-one
32	C15 H22 O3	(3R,3aR,4R,7R)-3,8,8-trimethyl-2-oxooctahydro-3a,7-ethanoindene-4-carboxylic acid
33	C15 H22 O3_b	(3R,3aR,4R,7R)-3,8,8-trimethyl-2-oxooctahydro-3a,7-ethanoindene-4-carboxylic acid
34	C15 H22 O3_c	(3S,4aR,5R,6R)-3,6-dihydroxy-4a,5-dimethyl-3-(prop-1-en-2-yl)-4,4a,5,6,7,8-hexahydronaphthalen-2(3H)-one
35	C15 H22 O3_d	6-hydroxy-4a-(hydroxymethyl)-5-methyl-3-(prop-1-en-2-yl)-4,4a,5,6,7,8-hexahydronaphthalen-2(3H)-one
36	C15 H24 O2	4-(hydroxymethyl)-3,4a,8,8-tetramethyl-4a,5,6,7,8,8a-hexahydronaphthalen-1(4H)-one
37	C15 H24 O3	6-hydroxy-4-(hydroxymethyl)-3,4a,8,8-tetramethyl-4a,5,6,7,8,8a-hexahydronaphthalen-1(4H)-one
38	C15 H24 O3_b	2-((2R,4aR,8R)-8-hydroxy-4a,8-dimethyldecahydronaphthalen-2-yl) acrylic acid
39	C15 H24 O3_c	1,4-dihydroxy-1,4-dimethyl-7-(propan-2-ylidene) octahydroazulen-6(2H)-one
40	C15 H26 O3	(1,6-dimethyl-1,2,3,4,4a,5,8,8a-octahydronaphthalene-1,4a,5-triyl) trimethanol
41	C15 H26 O5	2-(dec-9-en-1-yl)-3-hydroxypentanedioic acid

42	C16 H17 N O2	(S, Z)-N-(1-hydroxy-3-phenylpropan-2-yl) benzimidic acid
43	C16 H26 N6 O5 S	(S)-2-((S)-2-((S)-2,5-diamino-5-oxopentanamido)-4-(methyl thio) butan amido)-3-(1H-imidazol-4-yl) propanoic acid
44	C16 H26 N6 O5 S_b	(S)-2-((S)-5-amino-2-((S)-2-amino-4-(methyl thio) butan amido)-5-oxopentanamido)-3-(1H-imidazol-4-yl) propanoic acid
45	C16 H26 O3	(4Z,6E,10Z)-8-hydroxyhexadeca-4,6,10-trienoic acid
46	C16H26N6O5S	(S)-2-((S)-5-amino-2-((S)-2-amino-4-(methyl thio) butan amido)-5-oxopentanamido)-3-(1H-imidazol-4-yl) propanoic acid
47	C17 H14 N2 O2	(E)-3-benzylidene-4-methyl-3,4-dihydro-1H-benzo[e][1,4]diazepine-2,5-dione
48	C17 H33 N7 O4	6-amino-2-(1-(2-amino-5-guanidinopentanoyl) azetidine-2-carboxamido) hexanoic acid
49	C18 H22 O2	(13S)-3-hydroxy-13-methyl-7,8,9,11,12,13,15,16-octahydro-6H-cyclopenta[a]phenanthren-17(14H)-one
50	C18 H22 O2_b	(13S)-3-hydroxy-13-methyl-7,8,9,11,12,13,15,16-octahydro-6H-cyclopenta[a]phenanthren-17(14H)-one
51	C18 H22 O2_c	5,5'-dipropyl-[1,1'-biphenyl]-2,2'-diol
52	C18 H28 O3	8-((1S,5S)-4-oxo-5-((Z)-pent-2-en-1-yl) cyclopent-2-en-1-yl) octanoic acid
53	C18 H30 O3	(S,9Z,11E,15Z)-13-hydroxyoctadeca-9,11,15-trienoic acid
54	C18 H30 O3_b	(9Z,11E,15Z)-13-hydroxyoctadeca-9,11,15-trienoic acid
55	C18 H30 O3_c	(10E,12Z)-9-oxooctadeca-10,12-dienoic acid
56	C18 H30 O3_d	(10E,12Z,15Z)-9-hydroxyoctadeca-10,12,15-trienoic acid
57	C18 H32 O2	octadec-9-ynoic acid
58	C18 H32 O3	(10E,12E)-9-hydroxyoctadeca-10,12-dienoic acid
59	C18 H32 O3_b	(9E,11Z)-8-hydroxyoctadeca-9,11-dienoic acid
60	C18 H32 O4	(9Z,11E)-13-hydroperoxyoctadeca-9,11-dienoic acid
61	C18 H32 O4_b	(10Z,13Z)-15,16-dihydroxyoctadeca-10,13-dienoic acid
62	C18 H34 O4	8-hydroxy-8-(3-octyloxiran-2-yl) octanoic acid
63	C18 H34 O5	(Z)-9,10,11-trihydroxyoctadec-12-enoic acid
64	C18 H34 O5_b	(Z)-5,8,11-trihydroxyoctadec-9-enoic acid

Binding Affinities and Interaction Patterns

The docking results of the ligands isolated from the mushroom (A. asiaticus) extracts against the MmpL3 protein of M. tuberculosis demonstrate varied binding affinities and interaction patterns. Here, we analyze and compare these results, including the interactions of the known carboxamide derivatives (Ray et al., 2022), to evaluate the potential of these ligands as antitubercular agents (Figure 3). Out of all molecules, the ones with binding affinities between -6.5 to -8.7 were taken for further analyses.

ISSN PRINT 2319 1775 Online 2320 7876
 UGC CARE Listed (Group -I) Journal Volume 12, Iss 04, 2023

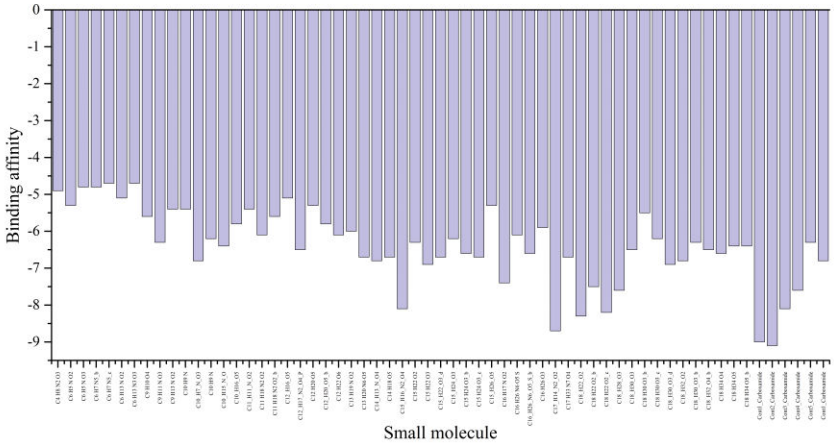

Figure 3 The binding affinity of small molecules from A. asiaticus with the MmpL3 protein of M. tuberculosis

The ligand **6-hydroxynicotinic acid ($C_6H_5NO_3$)** with the binding affinity of -6.1 interacts with the protein through multiple types of bonds. Conventional hydrogen bonds are observed with ILE (A:749), THR (A:284), and SER (A:647), indicating strong and specific interactions due to the hydrogen bonding. The Pi-Alkyl bond with ARG (A:283) suggests a hydrophobic interaction where the π-electrons of the aromatic ring interact with the alkyl side chain of the amino acid (Tewari & Dubey, 2008). These interactions collectively stabilize the ligand within the binding pocket of the protein, contributing to the overall binding affinity and specificity (Agnieszka K. Bronowska, 2006) (Figure 4-A).

The ligand **(E)-5-(4-methoxy-3-methyl-2-oxo-2H-pyran-6-yl)-3-methylhex-4-enoic acid; (3',4'-Dihydroinfectopyrone); ($C_{14}H_{18}O_5$)** with the binding affinity of -6.7, interacts with the protein through two types of bonds. The carbon hydrogen bond with HIS (A:234) suggests a moderate interaction involving the hydrogen attached to a carbon atom of the ligand (Power, 2011). The Pi-Alkyl bond with ILE (A:422) indicates a hydrophobic interaction where the π-electrons of the aromatic ring interact with the alkyl side chain of the amino acid. These interactions help stabilize the ligand within the binding pocket of the protein, contributing to the binding affinity and specificity (Figure 4-B).

The ligand **(3R,3aR,4R,7R)-3,8,8-trimethyl-2-oxooctahydro-3a,7-ethanoindene-4-carboxylic acid; (Dihydroterrecyclic acid), ($C_{15}H_{22}O_3$)** with the binding affinity of -6.9. The ligand interacts with the protein primarily through conventional hydrogen bonds. These bonds are with the amino acids ASN (A:513) and GLN (A:512). The bond lengths are 2.18 Å and 2.74 Å, respectively, indicating strong and specific interactions between the ligand and these amino acid residues. These hydrogen bonds are crucial for stabilizing the ligand within the binding pocket of the protein, contributing significantly to the binding affinity and specificity (Figure 4-C).

ISSN PRINT 2319 1775 Online 2320 7876
 UGC CARE Listed (Group -I) Journal Volume 12, Iss 04, 2023

The ligand **1,4-dihydroxy-1, 4-dimethyl-7-(propan-2-ylidene) octahydroazulen-6(2H)-one (Zedoarondiol); ($C_{15}H_{24}O_3$),** with the binding affinity of -6.7, interacts with the protein (MmpL3) through conventional hydrogen bonds and carbon hydrogen bonds. The conventional hydrogen bond with ASP (A:64) indicates a strong and specific interaction, with a bond length of 2.88 Å. This hydrogen bond is crucial for stabilizing the ligand within the binding pocket of the protein. The carbon hydrogen bond with GLY (A:67) suggests a moderate interaction involving the hydrogen attached to a carbon atom of the ligand, with a bond length of 3.51 Å. This interaction further contributes to the ligand's binding stability within the protein (Figure 4-D).

The ligand **(Z)-2-ethylidene-8, 11-dihydroxy-7-methoxy-2, 3-dihydro-1H-benzo [e] pyrrolo [1,2-a] [1,4] diazepin-5 (11aH)-one ($C_{15}H_{16}N_2O_4$)** with the binding affinity of -8.1, interacts with the protein (MmpL3) through various types of bonds, including conventional hydrogen bonds, carbon hydrogen bonds, Pi-Cation, and Pi-Alkyl interactions. Conventional hydrogen bonds are observed with GLN (A:437) at 2.09 Å, ARG (A:465) at 3.65 Å and 3.16 Å, and GLN (A:424) at 2.80 Å. These hydrogen bonds contribute to the strong and specific binding of the ligand within the protein's binding pocket. Carbon hydrogen bonds with ILE (A:422) at 3.63 Å suggest additional stabilization through moderate interactions involving hydrogen attached to a carbon atom of the ligand. Pi-Cation interaction with ARG (A:465) at 4.30 Å highlights the involvement of electrostatic interactions between the positive charge of the amino acid and the π-electrons of the aromatic ring in the ligand. Pi-Alkyl interactions with LEU (A:466) at 4.80 Å and 4.51 Å indicate hydrophobic interactions between the alkyl side chain of the amino acid and the π-electrons of the aromatic ring in the ligand. These interactions collectively stabilize the ligand within the protein's binding pocket, contributing to its binding affinity and specificity (Figure 4-E).

The ligand **(S, Z)-N-(1-hydroxy-3-phenylpropan-2-yl) benzimidic acid; (N-benzoyl phenylalaninol), ($C_{16}H_{17}NO_2$),** with the binding affinity of -7.4, interacts with the protein (MmpL3) through Pi-Sigma and Pi-Alkyl interactions, which are primarily hydrophobic interactions involving the aromatic rings and the side chains of the amino acids. Pi-Sigma interactions are observed with LEU (A:693) at 5.44 Å and LEU (A:173) at 3.93 Å, indicating interactions between the π-electrons of the aromatic ring in the ligand and the sigma bonds of the leucine side chains. Pi-Alkyl interactions are seen with ILE (A:422) at 5.08 Å, VAL (A:169) at 3.99 Å, and ALA (A:170) at 5.49 Å. These interactions involve the π-electrons of the aromatic rings in the ligand and the alkyl side chains of the amino acids. These hydrophobic interactions help stabilize the ligand within the binding pocket of the protein, contributing to the overall binding affinity and specificity (Figure 4-F).

ISSN PRINT 2319 1775 Online 2320 7876
 UGC CARE Listed (Group -I) Journal Volume 12, Iss 04, 2023

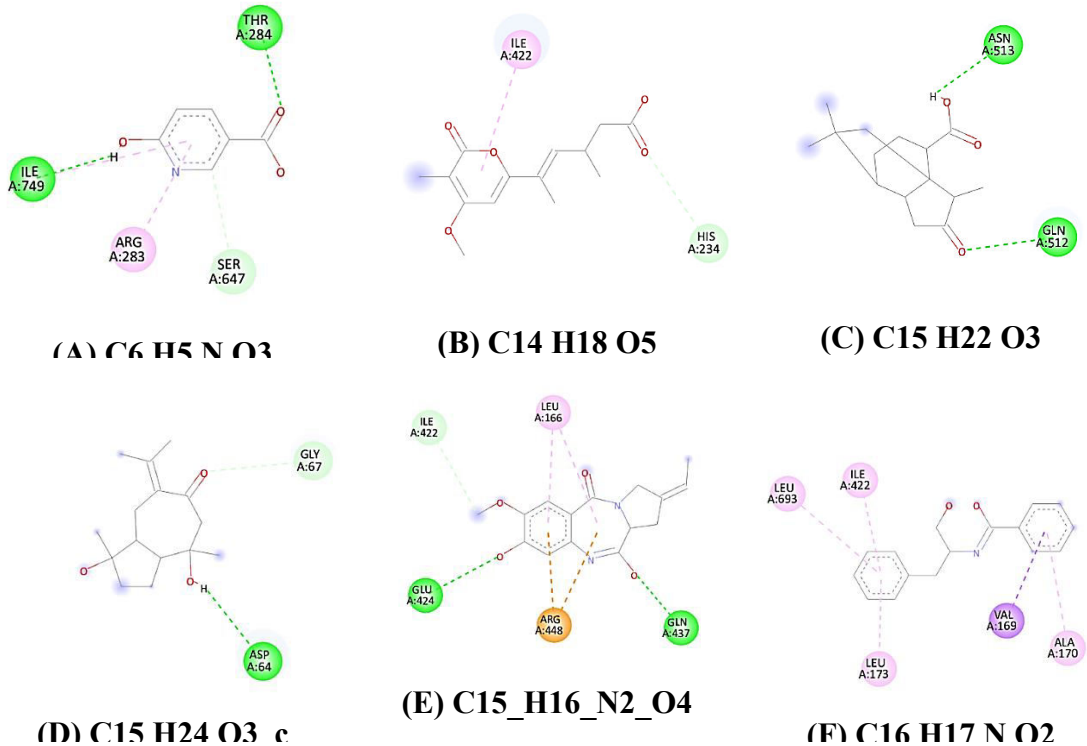

Figure 4 Interaction patterns of six different ligands with the macromolecule MmpL3. The figure illustrates the binding sites and interaction details for each ligand, highlighting key residues involved in the interactions.

The ligand **(E)-3-benzylidene-4-methyl-3, 4-dihydro-1H-benzo[e] [1,4] diazepine-2,5-dione; ((E)-dehydrocyclopeptine); ($C_{17}H_{14}N_2O_2$),** with the binding affinity of -8.7, interacts with the protein (MmpL3) through various types of bonds, including Pi-Anion, Pi-Pi Stacked, and Pi-Alkyl interactions. Pi-Anion interaction with ASP (A:139) at 5.27 Å indicates an electrostatic interaction between the negatively charged aspartate side chain and the π-electrons of the aromatic ring in the ligand. Pi-Pi Stacked interaction with LEU (A:166) at 3.91 Å highlights the involvement of aromatic stacking interactions between the aromatic rings of the ligand and the leucine side chain (Riley & Hobza, 2013). Pi-Alkyl interactions are observed with HIS (A:234) at 4.78 Å, ILE (A:173) at 5.18 Å, and ALA (A:170) at 4.79 Å and 5.01 Å. These interactions involve the π-electrons of the aromatic rings in the ligand and the alkyl side chains of the amino acids (Kumari et al., 2007). These interactions collectively stabilize the ligand within the protein's binding pocket, contributing to the binding affinity and specificity (Figure 5-A).

The ligand **(13S) – 3 – hydroxy – 13 – methyl - 7, 8, 9, 11, 12, 13, 15, 16 – octahydro - 6H – cyclopenta [a] phenanthrene - 17(14H) - one ($C_{18}H_{22}O_2$)** with the binding affinity of -7.5, interacts with the protein (MmpL3) through various types of interactions, including van der Waals interactions, conventional hydrogen bonds, amide-pi stacked interactions, alkyl interactions, and

pi-alkyl interactions. Van der Waals interactions with SER (A:46) suggest non-specific, weak interactions that contribute to the overall stabilization of the ligand. Conventional hydrogen bonds with ARG (A:465) at bond lengths of 2.25 Å and 1.99 Å indicate strong, specific interactions that are crucial for ligand binding. Amide-pi stacked interactions with PRO (A:138) at bond lengths of 4.10 Å and 4.94 Å highlight the involvement of stacking interactions between the amide group and the aromatic ring of the ligand. Alkyl interactions with ALA (A:499) at 4.83 Å and 5.15 Å, and with VAL (A:500), indicate hydrophobic interactions between the alkyl side chains of the amino acids and the ligand. Pi-alkyl interaction with ALA (A:499) further suggests hydrophobic interactions involving the π-electrons of the aromatic rings in the ligand and the alkyl side chains. (Figure 5-B).

The ligand **5,5'-dipropyl-[1,1'-biphenyl]-2,2'-diol; (Tetrahydromagnolol) ($C_{18}H_{22}O2$),** with the binding affinity of -8.2, interacts with the protein (MmpL3) through conventional hydrogen bonds, alkyl interactions, and Pi-Alkyl interactions. Conventional hydrogen bond with GLN (A:40) at 2.35 Å indicates a strong, specific interaction that is crucial for the ligand's binding. Alkyl interactions are observed with several amino acids: PHE (A:43) at 4.34 Å, ILE (A:422) at 4.22 Å, LEU (A:173) at 5.28 Å and 5.27 Å, LEU (A:693) at 4.95 Å, and MET (A:195) at 5.28 Å. These interactions involve the hydrophobic side chains of the amino acids and the ligand, contributing to the stabilization within the binding pocket. Pi-Alkyl interactions are seen with PHE (A:43) at 4.14 Å, ILE (A:422) at 4.72 Å, LEU (A:173) at 5.22 Å, and LEU (A:693) at 4.56 Å. These interactions involve the π-electrons of the aromatic rings in the ligand and the alkyl side chains of the amino acids, providing additional stabilization through hydrophobic interactions (Figure 5-C).

The ligand **8-hydroxy-8-(3-octyloxiran-2-yl) octanoic acid ($C_{18}H_{34}O_4$)** with the binding affinity of -6.6, interacts with the protein (MmpL3) through conventional hydrogen bonds, unfavourable acceptor-acceptor interactions, alkyl interactions, and Pi-Alkyl interactions. Conventional hydrogen bond with GLN (A:421) at 2.71 Å indicates a strong, specific interaction that is crucial for the ligand's binding. Unfavourable acceptor-acceptor interaction with ASP (A:231) at 2.71 Å suggests a repulsive interaction that may slightly destabilize the binding (Martin et. al., 2000). Alkyl interactions are observed with several amino acids: PHE (A:43) at 5.18 Å, ILE (A:422) at 4.44 Å, LEU (A:173) at 4.51 Å and 4.56 Å, LEU (A:693) at 4.65 Å, PHE (A:226) at 4.37 Å, and TYR (A:424) at 5.44 Å. These interactions involve the hydrophobic side chains of the amino acids and the ligand, contributing to stabilization within the binding pocket. Pi-Alkyl interactions are seen with PHE (A:43) at 5.49 Å, ILE (A:422) at 4.44 Å and 5.18 Å, LEU (A:693) at 4.65 Å and 5.25 Å, and LEU (A:173) at 4.51 Å. These interactions involve the π-electrons of the aromatic rings in the ligand and the alkyl side chains of the amino acids, providing additional stabilization through hydrophobic interactions. These interactions collectively stabilize the ligand within the protein's binding pocket, enhancing the binding affinity and specificity, although the unfavourable acceptor-acceptor interaction might slightly counteract some of this stability (Figure 5-D).

ISSN PRINT 2319 1775 Online 2320 7876
 UGC CARE Listed (Group -I) Journal Volume 12, Iss 04, 2023

The ligand **(13S) – 3 – hydroxy – 13 – methyl - 7, 8, 9, 11, 12, 13, 15, 16 – octahydro - 6H – cyclopenta [a] phenanthrene – 17 (14H) - one ($C_{18}H_{22}O_2$)** with the binding affinity of -8.3, interacts with the protein (MmpL3) through alkyl and Pi-Alkyl interactions: Alkyl interactions are observed with ALA (A:170) at 4.85 Å and LEU (A:173) at 5.31 Å. These interactions involve the hydrophobic side chains of the amino acids and the ligand, contributing to the stabilization within the binding pocket. Pi-Alkyl interactions are seen with LEU (A:173) at 5.69 Å and 5.31 Å, and ILE (A:422) at 5.31 Å. These interactions involve the π-electrons of the aromatic rings in the ligand and the alkyl side chains of the amino acids, providing additional stabilization through hydrophobic interactions (Figure 5-E).

Ligand **8-((1S,5S) – 4 – oxo – 5 - ((Z) – pent – 2 – en – 1 - yl) cyclopent – 2 – en – 1 - yl) octanoic acid; (12-Oxo-phytodienoic acid); ($C_{18}H_{28}O_3$)**, with the binding affinity of -7.6 interacts with the protein (MmpL3) through various types of interactions, including unfavourable acceptor-acceptor, alkyl, and Pi-Alkyl interactions. Unfavourable acceptor-acceptor interaction with SER (A:551) at 2.83 Å suggests a repulsive interaction that may slightly destabilize the binding. Alkyl interactions are observed with ILE (A:422) at 3.87 Å, PHE (A:236) at 4.76 Å and 4.98 Å, and TYR (A:235) at 5.45 Å. These interactions involve the hydrophobic side chains of the amino acids and the ligand, contributing to stabilization within the binding pocket. Pi-Alkyl interactions are seen with ILE (A:177) at 4.67 Å, HIS (A:234) at 5.21 Å, LEU (A:693) at 4.97 Å, PHE (A:44) at 4.28 Å and 4.52 Å, and TYR (A:44) at 4.52 Å. These interactions involve the π-electrons of the aromatic rings in the ligand and the alkyl side chains of the amino acids, providing additional stabilization through hydrophobic interactions. These interactions collectively stabilize the ligand within the protein's binding pocket, enhancing the binding affinity and specificity, however the unfavourable acceptor-acceptor interaction might slightly counteract some of this stability (Figure 5-F).

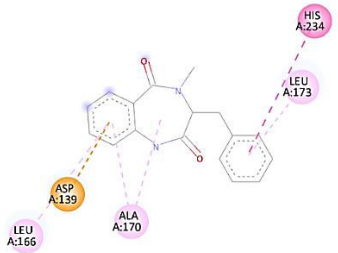

(A) C17_H14_N2_O2

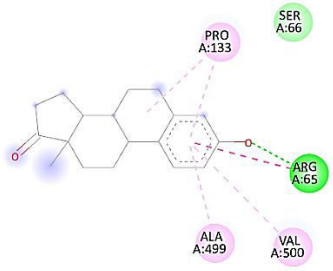

(B) C18 H22 O2_b

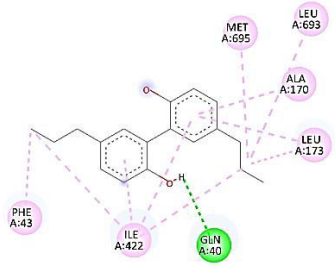

(C) C18 H22 O2_c

ISSN PRINT 2319 1775 Online 2320 7876
 UGC CARE Listed (Group -I) Journal Volume 12, Iss 04, 2023

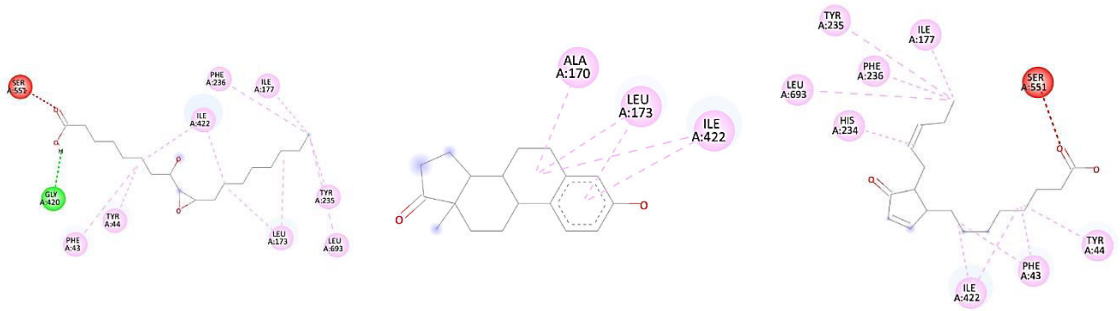

(D) C18 H34 O4 **(E) C18_H22_O2** **(F) C18_H28_O3**

Figure 5 Interaction patterns of six different ligands with the macromolecule MmpL3. The figure illustrates the binding sites and interaction details for each ligand, highlighting key residues involved in the interactions.

The ligand **(10E,12Z,15Z)-9-hydroxyoctadeca-10,12,15-trienoic acid ($C_{18}H_{30}O_3$)** with the binding affinity of -6.9, interacts with the protein (MmpL3) through conventional hydrogen bonds, carbon hydrogen bonds, alkyl interactions, and Pi-Alkyl interactions. Conventional hydrogen bonds are observed with SER (A:551) at 2.31 Å and PHE (A:41) at 2.43 Å, indicating strong and specific interactions that are crucial for ligand binding. Carbon hydrogen bond with ASP (A:139) at 3.46 Å suggests additional stabilization through moderate interactions involving hydrogen attached to a carbon atom of the ligand. Alkyl interactions are observed with LEU (A:173) at 4.64 Å, ILE (A:177) at 4.29 Å, LEU (A:693) at 4.46 Å, and PHE (A:236) at 4.44 Å. These interactions involve the hydrophobic side chains of the amino acids and the ligand, contributing to stabilization within the binding pocket. Pi-Alkyl interactions are seen with ILE (A:422) at 5.09 Å, PHE (A:41) at 4.41 Å, TYR (A:40) at 4.64 Å and 4.83 Å, LEU (A:693) at 4.46 Å, TYR (A:235) at 5.02 Å, PHE (A:236) at 4.79 Å, and ILE (A:177) at 4.44 Å. These interactions involve the π-electrons of the aromatic rings in the ligand and the alkyl side chains of the amino acids, providing additional stabilization through hydrophobic interactions (Figure 6-A).

The ligand **3-methyl-N-(4-methylcyclohexyl)-1H-indole-2-carboxamide** interacts with the protein MmpL3 with a binding affinity of -9, indicating strong binding interactions. The ligand establishes various types of non-covalent interactions with the protein residues, contributing to its stabilization within the binding pocket. Conventional hydrogen bond formation is observed with GLN (A:40) at a distance of 1.98 Å, indicating a strong and specific interaction that is crucial for ligand binding. Pi-anion interactions occur with ASP (A:139) at distances of 3.77 Å and 4.36 Å, suggesting additional stabilization through electrostatic interactions between the π-electrons of the aromatic ring in the ligand and the negatively charged carboxylate group of Aspartate. A pi-sigma bond is formed with VAL (A:169) at a distance of 3.57 Å, indicating interaction between the π-electrons of the aromatic ring in the ligand and the σ-electrons of the valine side chain. An alkyl interaction is observed with LEU (A:173) at a distance of 4.76 Å, involving the hydrophobic side chain of LEU and the ligand, contributing to hydrophobic stabilization within the binding pocket.

ISSN PRINT 2319 1775 Online 2320 7876
 UGC CARE Listed (Group -I) Journal Volume 12, Iss 04, 2023

Pi-alkyl interactions are seen with LEU (A:166) at a distance of 5.39 Å, involving the π-electrons of the aromatic ring in the ligand and the alkyl side chain of leucine, providing additional stabilization through hydrophobic interactions. These interactions collectively contribute to the high binding affinity and stability of the ligand within the binding pocket of the protein MmpL3 (Figure 6-B).

The ligand **3-(benzyl amino)-N-cyclohexyl-1H-indole-2-carboxamide** interacts with the protein MmpL3 with a binding affinity of -9.1, indicating strong binding interactions. The ligand establishes various types of non-covalent interactions with the protein residues, contributing to its stabilization within the binding pocket. Conventional hydrogen bond formation is observed with GLN (A:40) at a distance of 2.06 Å, indicating a strong and specific interaction that is crucial for ligand binding. A carbon hydrogen bond is observed with GLU (A:424) at a distance of 3.42 Å, suggesting additional stabilization through moderate interactions involving a hydrogen attached to a carbon atom of the ligand. Pi-sigma interactions occur with VAL (A:169) at a distance of 3.82 Å and ILE (A:422) at a distance of 3.69 Å, indicating interaction between the π-electrons of the aromatic ring in the ligand and the σ-electrons of the VAL and ILE side chains. Alkyl interactions are observed with VAL (A:169) at a distance of 3.67 Å and ILE (A:422) at a distance of 4.59 Å, involving the hydrophobic side chains of these amino acids and the ligand, contributing to hydrophobic stabilization within the binding pocket. Pi-alkyl interactions are seen with ALA (A:170) at a distance of 5.24 Å and LEU (A:173) at a distance of 4.62 Å, involving the π-electrons of the aromatic ring in the ligand and the alkyl side chains of alanine and leucine, providing additional stabilization through hydrophobic interactions. These interactions collectively contribute to the high binding affinity and stability of the ligand within the binding pocket of the protein MmpL3 (Figure 6-C).

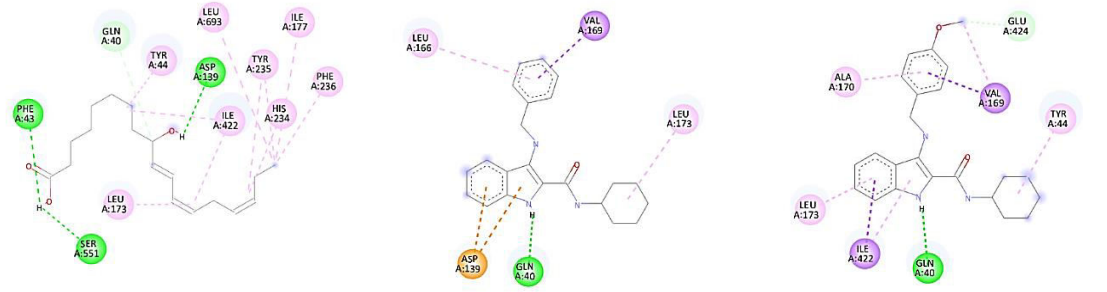

(A) C18_H30_O3 **(B) 3-Methyl-N-(4-** **(C) 3-(Benzyl amino)-N-**

Figure 6 Interaction patterns of one sample ligand and two control ligands with the macromolecule MmpL3. The figure illustrates the binding sites and interaction details for each ligand, highlighting key residues involved in the interactions.

ISSN PRINT 2319 1775 Online 2320 7876
 UGC CARE Listed (Group -I) Journal Volume 12, Iss 04, 2023

Drug-likeness and pharmacokinetic properties:

The test samples exhibit physicochemical properties with molecular weights ranging from low (139) to moderate (314), similar to the known samples (Figure 7 A). The fraction of sp3 hybridized carbons indicates a balance between rigidity and flexibility, with higher values suggesting better bioavailability (Rossi Sebastiano et al., 2018). Moderate TPSA values are favorable for cell membrane permeability (Rastogi & Jana, 2016). Lipophilicity, as indicated by Log Po/w, shows moderate values suggesting a good balance between solubility and membrane permeability, however very high or low values may require formulation challenges (Supriyo & Dilipkumar, 2017) (Figure 7 B). Water solubility, assessed through Log S (ESOL, Ali, SILICOS-IT), shows variations across models, necessitating experimental validation due to its impact on absorption and distribution. High gastrointestinal absorption is favorable for oral drugs, while blood-brain barrier permeability suggests potential CNS activity. The lack of Cytochrome P450 enzyme inhibition indicates a lower risk of drug-drug interactions (Deodhar et al., 2020), and low skin permeation (Log Kp) values are common among the samples. Compliance with Lipinski's Rule of Five indicates potential for oral bioavailability, with bioavailability scores ranging from moderate to high (0.55 to 0.85) (Figure 7 C). Medicinal chemistry assessments reveal a lack of PAINS and Brenk alerts, suggesting fewer false positives and problematic substructures, and synthetic accessibility scores indicate that the compounds are reasonably easy to synthesize (Figure 7 D).

These findings on the bioactive compounds of A. asiaticus and their potential antituberculosis properties resonate with previous research on A. odoratus (Arpha et al., 2012). and the critical role of the MmpL3 protein in M. tuberculosis pathogenesis (Bolla, 2020). Similar to our identification of 64 metabolites from A. asiaticus showing various binding affinities to the MmpL3 protein. These findings collectively highlight the potential of Astraeus species as promising sources of novel antituberculosis agents and support the ongoing exploration of natural products for safer and more effective TB treatments.

ISSN PRINT 2319 1775 Online 2320 7876
 UGC CARE Listed (Group -I) Journal Volume 12, Iss 04, 2023

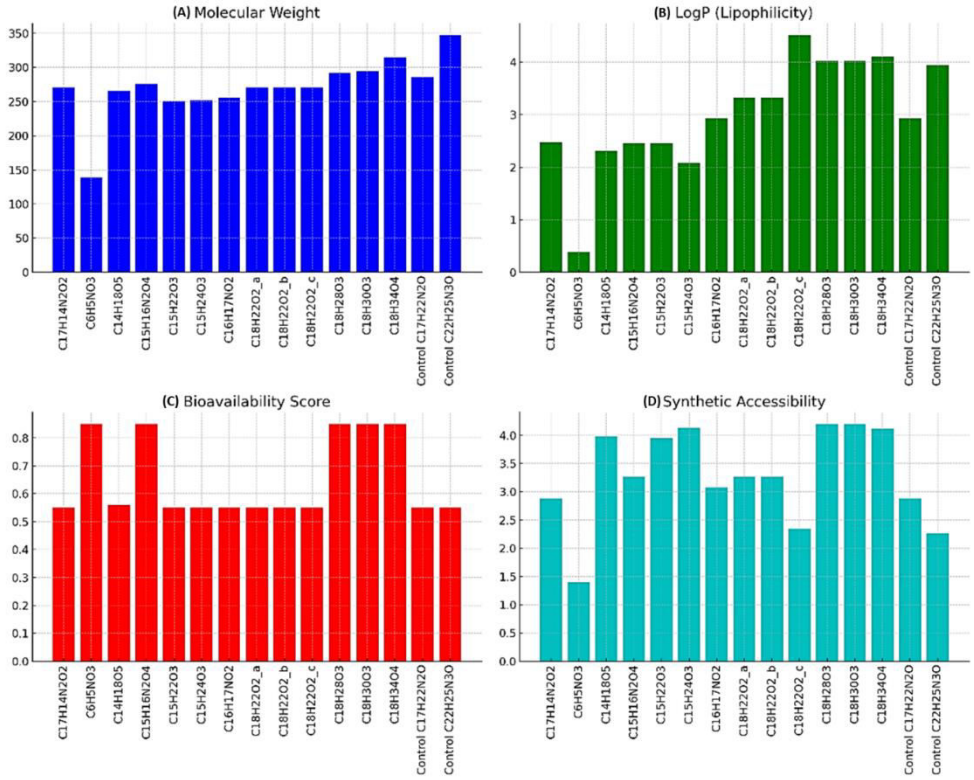

Figure 7 Graphical representation of key parameters for the test samples: (A) Molecular Weight, (B) Log Po/w (Lipophilicity), (C) Bioavailability Score, and (D) Synthetic Accessibility Score.

Conclusion

The current study demonstrates the significant potential of metabolites extracted from the mushroom A. asiaticus as antituberculosis agents, particularly against the MmpL3 protein of M. tuberculosis. Out of the 64 metabolites analyzed, several small molecules exhibited promising binding affinities and stability, comparable to known carboxamide derivatives. Notably, compounds such as (3R,3aR,4R,7R)-3,8,8-trimethyl-2-oxooctahydro-3a,7-ethanoindene-4-carboxylic acid (C15H22O3), (Z)-2-ethylidene-8,11-dihydroxy-7-methoxy-2,3-dihydro-1H-benzo[e]pyrrolo[1,2-a][1,4]diazepin-5(11aH)-one (C15H16N2O4), (S,Z)-N-(1-hydroxy-3-phenylpropan-2-yl) benzimidic acid (C16H17NO2), (E)-3-benzylidene-4-methyl-3,4-dihydro-1H-benzo[e][1,4]diazepine-2,5-dione (C17H14N2O2), (13S)-3-hydroxy-13-methyl-7,8,9,11,12,13,15,16-octahydro-6H-cyclopenta[a]phenanthrene-17(14H)-one (C18H22O2), 5,5'-dipropyl-[1,1'-biphenyl]-2,2'-diol (C18H22O2), (10E,12Z,15Z)-9-hydroxyoctadeca-10,12,15-trienoic acid (C18H30O3), and others have shown good binding affinity and stability with the MmpL3 protein.

Moreover, these molecules displayed favorable drug-likeness properties, suggesting their potential as viable candidates to be developed as antituberculosis agents. The high binding affinity and

stability of these compounds highlight the potential of A. asiaticus as a natural source for novel antituberculosis agents targeting the MmpL3 protein.

In conclusion, this study provides a direction for the exploration of natural products, specifically mushroom-derived compounds, in the search for new therapeutic strategies against TB. The promising results of the A. asiaticus metabolites underscore the importance of natural sources in drug discovery and the ongoing need for innovative approaches to combat drug-resistant TB. Further work should focus on the in-vitro biological evaluation of these compounds and their potential synergistic effects with existing TB treatments to fully understand their therapeutic potential.

Acknowledgments: All the authors are thankful to Pt. Ravishankar Shukla University, Raipur, C.G. India, for providing laboratory facilities, and also thankful to the Department of Biotechnology (DBT) for sponsoring the project (BT/PR29526/FcB/125/16/2018) and providing instrumentation facilities.

Conflicts of Interest: The authors declare no conflict of interest.

Reference

Agnieszka K. Bronowska. (2006). Thermodynamics of Ligand-Protein Interactions: Implications for Molecular Design. Thermodynamics - Interaction Studies - Solids, Liquids and Gases. Breast Diseases, 17(2).

Al-obaidy, A., & Esmaeel, F. (2021). Effect of Saussurea costus extracts in the viability of Echinococcus granulosus protoscoleces of sheep origin In vitro. JOURNAL OF EDUCATION AND SCIENCE, 30(3). https://doi.org/10.33899/edusj.2021.168656

Arpha, K., Phosri, C., Suwannasai, N., Mongkolthanaruk, W., & Sodngam, S. (2012). Astraodoric acids A-D: New lanostane triterpenes from edible mushroom astraeus odoratus and their anti-mycobacterium tuberculosis H37Ra and cytotoxic activity. Journal of Agricultural and Food Chemistry, 60(39), 9834–9841. https://doi.org/10.1021/JF302433R/SUPPL_FILE/JF302433R_SI_001.PDF

Azam, S. S., Abro, A., & Raza, S. (2015). Binding pattern analysis and structural insight into the inhibition mechanism of Sterol 24-C methyltransferase by docking and molecular dynamics approach. Journal of Biomolecular Structure and Dynamics, 33(12). https://doi.org/10.1080/07391102.2014.1002423

Baye, A. M., Demisis Sarhie, W., & Endalew, B. T. (2018). Treatment Outcomes of Multi-Drug-Resistant Tuberculosis and Its Determinants in Boru Meda Hospital, Northeast Ethiopia. Journal of Infectious Diseases & Therapy, 06(01). https://doi.org/10.4172/2332-0877.1000350

Bendre, A. D., Peters, P. J., & Kumar, J. (2021). Tuberculosis: Past, present and future of the treatment and drug discovery research. In Current Research in Pharmacology and Drug Discovery (Vol. 2). https://doi.org/10.1016/j.crphar.2021.100037

Biswas, G., Nandi, S., Kuila, D., & Acharya, K. (2017). A comprehensive review on food and medicinal prospects of astraeus hygrometricus. Pharmacognosy Journal, 9(6). https://doi.org/10.5530/pj.2017.6.125

Bolla, J. R. (2020). Targeting MmpL3 for anti-tuberculosis drug development. In Biochemical Society Transactions (Vol. 48, Issue 4). https://doi.org/10.1042/BST20190950

Dallakyan, S., & Olson, A. J. (2015). Small-molecule library screening by docking with PyRx. Methods in Molecular Biology, 1263. https://doi.org/10.1007/978-1-4939-2269-7_19

Deodhar, M., Al Rihani, S. B., Arwood, M. J., Darakjian, L., Dow, P., Turgeon, J., & Michaud, V. (2020). Mechanisms of cyp450 inhibition: Understanding drug-drug interactions due to mechanism-based inhibition in clinical practice. In Pharmaceutics (Vol. 12, Issue 9). https://doi.org/10.3390/pharmaceutics12090846

Jejurikar, B. L., & Rohane, S. H. (2021). Drug Designing in Discovery Studio. Asian J. Research Chem, 14(2).

Kumari, S., Prabhakar, S., Vairamani, M., Lavanya Devi, C., Chaitanya, G. K., & Bhanuprakash, K. (2007). Chiral Discrimination of D- and L-Amino Acids Using Iodinated Tyrosines as Chiral References: Effect of Iodine Substituent. Journal of the American Society for Mass Spectrometry, 18(8). https://doi.org/10.1016/j.jasms.2007.05.006

Lakshmipathy, G. (2013). Studies on different drying, canning and value addition techniques for mushrooms (Calocybe Indica). African Journal of Food Science, 7(10). https://doi.org/10.5897/ajfs2013.1002

Li, W., Obregón-Henao, A., Wallach, J. B., North, E. J., Lee, R. E., Gonzalez-Juarrero, M., Schnappinger, D., & Jackson, M. (2016). Therapeutic potential of the Mycobacterium tuberculosis mycolic acid transporter, MmpL3. Antimicrobial Agents and Chemotherapy, 60(9). https://doi.org/10.1128/AAC.00826-16

Liang, F., Tantan, R., Peize, Z., & Shuihua, L. (2023). Interpretation of WHO consolidated guidelines on tuberculosis, Module 4 ：treatment-drug-resistant tuberculosis treatment, 2022 update. Chinese Journal of Antituberculosis, 45(4). https://doi.org/10.19982/j.issn.1000-6621.20220523

Parida, S. K., Axelsson-Robertson, R., Rao, M. V., Singh, N., Master, I., Lutckii, A., Keshavjee, S., Andersson, J., Zumla, A., & Maeurer, M. J. (2015). Totally drug-resistant tuberculosis and adjunct therapies. In Journal of Internal Medicine (Vol. 277, Issue 4). https://doi.org/10.1111/joim.12264

Power, P. P. (2011). Interaction of multiple bonded and unsaturated heavier main group compounds with hydrogen, ammonia, olefins, and related molecules. Accounts of Chemical Research, 44(8). https://doi.org/10.1021/ar2000875

Rastogi, H., & Jana, S. (2016). Evaluation of physicochemical properties and intestinal permeability of six dietary polyphenols in human intestinal colon adenocarcinoma Caco-2 cells. European Journal of Drug Metabolism and Pharmacokinetics, 41(1). https://doi.org/10.1007/s13318-014-0234-5

Ray, R., Birangal, S. R., Fathima, F., Boshoff, H. I., Forbes, H. E., Hariharapura, R. C., & Shenoy, G. G. (2022). Molecular insights into Mmpl3 lead to the development of novel indole-2-carboxamides as antitubercular agents. Molecular Systems Design and Engineering, 7(6). https://doi.org/10.1039/d1me00122a

Rayasam, G. V. (2014). MmpL3 a potential new target for development of novel anti-tuberculosis drugs. In Expert Opinion on Therapeutic Targets (Vol. 18, Issue 3). https://doi.org/10.1517/14728222.2014.859677

Riley, K. E., & Hobza, P. (2013). On the importance and origin of aromatic interactions in chemistry and biodisciplines. Accounts of Chemical Research, 46(4). https://doi.org/10.1021/ar300083h

Rossi Sebastiano, M., Doak, B. C., Backlund, M., Poongavanam, V., Over, B., Ermondi, G., Caron, G., Matsson, P., & Kihlberg, J. (2018). Impact of Dynamically Exposed Polarity on Permeability and Solubility of Chameleonic Drugs beyond the Rule of 5. Journal of Medicinal Chemistry, 61(9). https://doi.org/10.1021/acs.jmedchem.8b00347

Sarathy, J. P., Ganapathy, U. S., Zimmerman, M. D., Dartois, V., Gengenbacher, M., & Dick, T. (2020). TBAJ-876, a 3,5-dialkoxypyridine analogue of bedaquiline, is active against Mycobacterium abscessus. Antimicrobial Agents and Chemotherapy, 64(4). https://doi.org/10.1128/AAC.02404-19

Silva, D. R., Dalcolmo, M., Tiberi, S., Arbex, M. A., Munoz-Torrico, M., Duarte, R., D'Ambrosio, L., Visca, D., Rendon, A., Gaga, M., Zumla, A., & Migliori, G. B. (2018). New and repurposed drugs to treat multidrug- and extensively drug-resistant tuberculosis. In Jornal Brasileiro de Pneumologia (Vol. 44, Issue 2). https://doi.org/10.1590/s1806-37562017000000436

Sun, Q., Li, S., Bai, X., Fu, J., Wang, G., Meng, D., & He, C. (2016). Analysis of characteristics and quality of hot air drying edible fungus. 2016 American Society of Agricultural and Biological Engineers Annual International Meeting, ASABE 2016. https://doi.org/10.13031/aim.20162460069

Supriyo, S., & Dilipkumar, P. (2017). Encyclopedia of physical organic chemistry. Encyclopedia of Physical Organic Chemistry, 6(April).

ISSN PRINT 2319 1775 Online 2320 7876
 UGC CARE Listed (Group -I) Journal Volume 12, Iss 04, 2023

Tan, L. P., Hamdan, R. H., Mohamed, M., Choong, S. S., Chan, Y. Y., & Lee, S. H. (2018). Antibacterial activity and toxicity of Duckweed, Lemna minor L. (Arales: Lemnaceae) from Malaysia. Malaysian Journal of Microbiology, 14(5). https://doi.org/10.21161/mjm.114417

Tewari, A. K., & Dubey, R. (2008). Emerging trends in molecular recognition: Utility of weak aromatic interactions. In Bioorganic and Medicinal Chemistry (Vol. 16, Issue 1). https://doi.org/10.1016/j.bmc.2007.09.023

Theuretzbacher, U., Outterson, K., Engel, A., & Karlén, A. (2020). The global preclinical antibacterial pipeline. In Nature Reviews Microbiology (Vol. 18, Issue 5). https://doi.org/10.1038/s41579-019-0288-0

Traoré, A. N., Rikhotso, M. C., Banda, N. T., Mashilo, M. S., Ngandu, J. P. K., Mavumengwana, V., Loxton, A. G., Kinnear, C., Potgieter, N., Heysell, S., & Warren, R. (2022). Effectiveness of the Novel Anti-TB Bedaquiline against Drug-Resistant TB in Africa: A Systematic Review of the Literature. In Pathogens (Vol. 11, Issue 6). https://doi.org/10.3390/pathogens11060636

Wang, A., Lu, Y., Lv, K., Ma, C., Xu, S., Wang, B., Wang, A., Xia, G., & Liu, M. (2020). Design, synthesis and antimycobacterial activity of new benzothiazinones inspired by rifampicin/rifapentine. Bioorganic Chemistry, 102. https://doi.org/10.1016/j.bioorg.2020.104135